

# Single top quark production in the $t$ -channel at 14 TeV and 33 TeV

Brad Schoenrock,<sup>1</sup> Elizabeth Drueke,<sup>1</sup> Barbara  
Alvarez Gonzalez,<sup>1</sup> and Reinhard Schwienhorst<sup>1</sup>

<sup>1</sup>*Department of Physics and Astronomy,  
Michigan State University, East Lansing MI 48824, USA*

(Dated: July 4, 2018)

## Abstract

We study  $t$ -channel single top quark production at future LHC runs at 14 TeV with  $300 \text{ fb}^{-1}$  and  $3000 \text{ fb}^{-1}$  as well as at a future 33 TeV proton-proton collider in the context of the Snowmass 2013 study. The single top final state has a lepton and neutrino from the top quark decay plus two jets, one of which is required to be  $b$ -tagged. We show that it is possible to isolate large samples of single top events and that the cross-section can be measured with a precision of 5% or better.

PACS numbers: 14.65.Ha, 12.15.-y

## 1 I. INTRODUCTION

2 The Large Hadron Collider (LHC) is the highest-energy particle accelerator ever built,  
3 probing physics at the TeV scale. The Higgs boson discovery [1, 2] was the first, but  
4 more discoveries are likely at the LHC which covers the energy range where new physics is  
5 anticipated.

6 Single top quarks are produced in the Standard Model (SM) through three different  
7 mechanisms: the  $t$ -channel exchange of a  $W$  boson, the corresponding Feynman diagram is  
8 shown in Fig. 1, the associated production of an on-shell  $W$  boson and a top-quark, and the  
9  $s$ -channel production and decay of a virtual  $W$  boson.

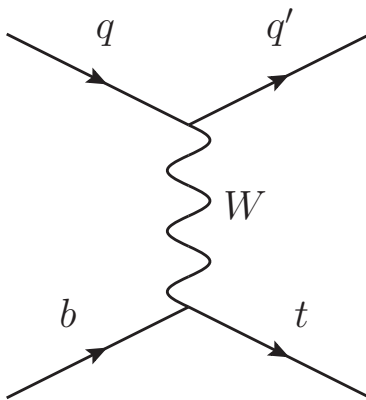


FIG. 1: Leading order Feynman diagram for single top quark production in the  $t$ -channel.

10 The single top quark discovery has been reported by the Tevatron experiments [3–5],  
11 based on a combination of  $t$ -channel and  $s$ -channel processes in 2009. The  $t$ -channel process  
12 has been observed at the Tevatron [6, 7] and at the 7 TeV LHC by ATLAS [8] and CMS [9,  
13 10]. The current precision of the  $t$ -channel cross-section measurements at 8 TeV performed  
14 by ATLAS [11] and CMS [12] is about 15%. Work is in progress to update these results  
15 with the full 2012 8 TeV dataset.

16 In this paper we explore the precision with which it will be possible to measure the single  
17 top quark production cross-section in the  $t$ -channel for three different scenarios:  $300 \text{ fb}^{-1}$  of  
18 14 TeV data with an average pileup of 50 events, also known as the Phase-1 running of the  
19 LHC upgrade;  $3000 \text{ fb}^{-1}$  of 14 TeV data with an average pileup of 140 events, also known  
20 as Phase-2 running or the high-luminosity LHC (HL-LHC); and  $3000 \text{ fb}^{-1}$  of 33 TeV data  
21 with an average pileup of 140 events, also known as the high-energy LHC (HE-LHC). For

22 each scenario we use the appropriate Snowmass detector model. The analysis is performed  
 23 using a simple cut-based approach to extract the  $t$ -channel signal. It is tuned to get at least  
 24 a signal to background ratio of five in order to obtain a clean sample of  $t$ -channel single-top  
 25 events.

26 This paper is organized as follows: Section II describes the Monte Carlo samples that  
 27 are used for this analysis. Section III explains the event selection and the analysis strategy.  
 28 Section IV shows the final event selection and Section V gives our conclusions.

## 29 II. SIGNAL AND BACKGROUND MODELING

30 The signal  $t$ -channel events are generated with Madgraph5 [13, 14], with Pythia8 [15, 16]  
 31 for parton showering and Delphes [17] for modeling of the Snowmass LHC detector [18]. We  
 32 consider inclusive  $t$ -channel events  $\bar{b} t$  and  $b \bar{t}$  and no attempt is made to separate top from  
 33 antitop.

34 Background samples for  $W/\gamma/Z$ +Jets, diboson,  $t\bar{t}$ , and  $Wt$  single top are used from the  
 35 official Snowmass webpage [18]. These samples are generated in bins of  $H_T$ , each with its  
 36 own cross-section. Normalizations are made according to the cross-sections provided by the  
 37 Snowmass site for the background samples and according to the leading order cross-sections  
 38 provided by MadGraph for the signal samples. The total cross-section for the signal and  
 39 backgrounds at 14 TeV and 33 TeV are listed in Table I and II, respectively.

Sample	Cross-Section [pb]
t-channel	30.2
$W$ +jets	238400
$t\bar{t}$	578.5
Diboson	289.8
$Wt$	72.1

TABLE I: cross-sections for each background sample at 14 TeV.

Sample	Cross-Section [pb]
t-channel	493.5
$W$ +jets	674860.6
$t\bar{t}$	4014.8
Diboson	894.0
$Wt$	492.6

TABLE II: cross-sections for each background sample at 33 TeV.

### 40 III. ANALYSIS

41 For this analysis a cut-and-count method is used. To account for differences in generation,  
42 select the relevant event signature, and to provide object definitions the following basic event  
43 selection is applied, on which subsequent steps are based:

$$\begin{aligned}
\text{One lepton (electron or muon) with} & \quad p_T^\ell \geq 40 \text{ GeV}, & |\eta_\ell| \leq 2.5, \\
\text{Two jets with} & \quad p_T^j \geq 70 \text{ GeV}, & |\eta_j| \leq 4.5, \\
\text{One b-jet with} & \quad p_T^j \geq 70 \text{ GeV}, & |\eta_j| \leq 2.5, \\
\text{Missing energy} & \quad \cancel{E}_T \geq 30 \text{ GeV}
\end{aligned}
\tag{1}$$

44 where  $p_T^\ell$  and  $\eta_\ell$  correspond to the transverse momentum and pseudorapidity of the lepton,  
45 respectively, and  $p_T^j$  and  $\eta_j$  are the transverse momentum and pseudorapidity of each jet.  
46 For 33 TeV  $p_T^\ell \geq 50$  GeV and  $p_T^j \geq 75$  GeV are used.

47 The first line in tables III, IV and V give the expected event yields for the signal and  
48 backgrounds with basic event selection for the different scenarios. At this stage the ratio of  
49 the signal contribution over the total background is about 0.13, with  $t\bar{t}$  being the dominant  
50 background contribution.

51 Figure 2 shows some kinematic distributions after the preselection cuts are applied. The  
52 contributions are broken into the  $t$ -channel single top signal events, other top events that  
53 correspond with  $Wt$  and  $t\bar{t}$ , and other backgrounds that come from  $W$ +jets and diboson  
54 events (labeled as Boson on the plots). The expected events are normalized using the  
55 14 TeV reference cross-sections and the integrated luminosity of  $300 \text{ fb}^{-1}$ . The distributions

for 33 TeV are shown in Figure 3.

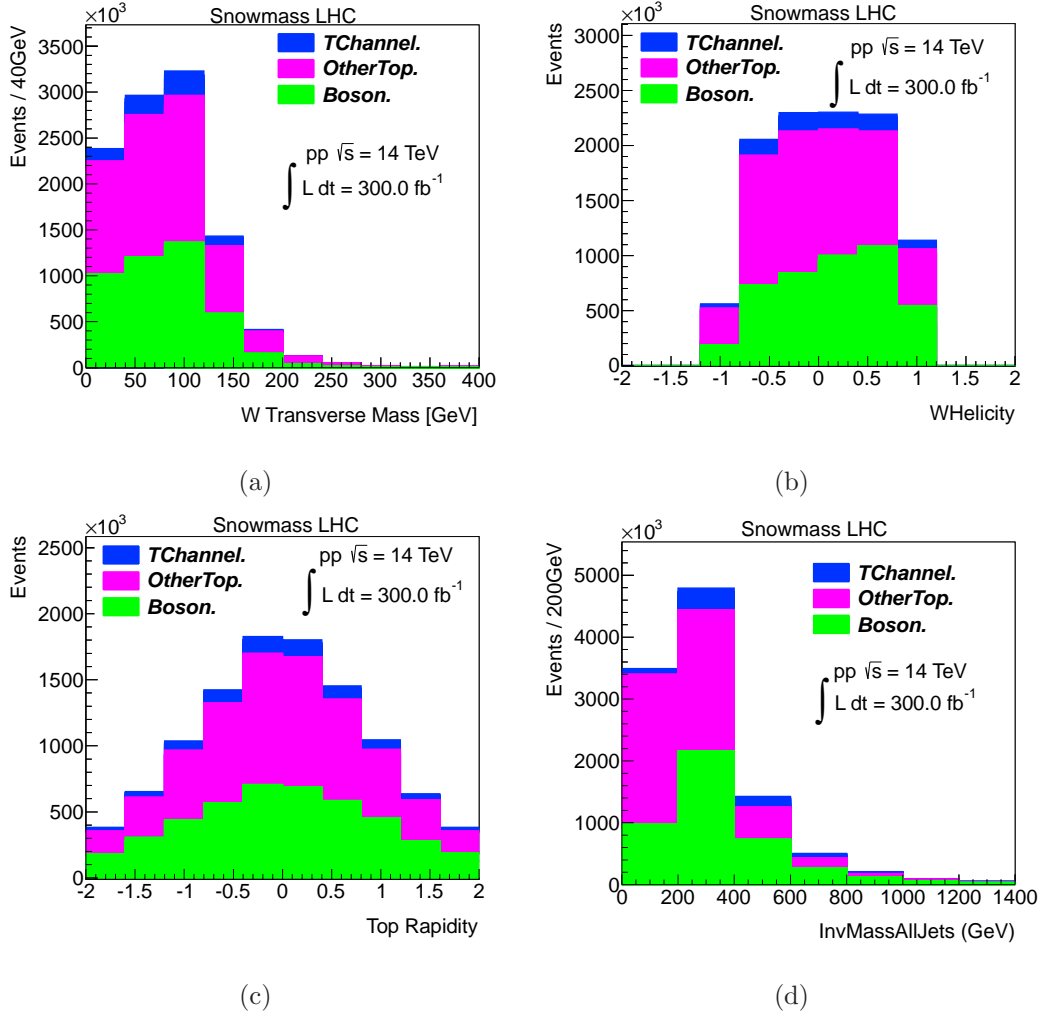
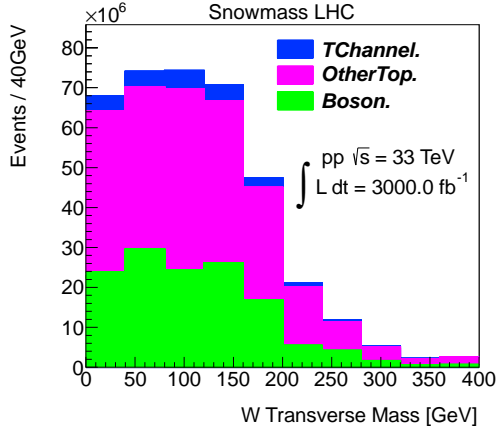
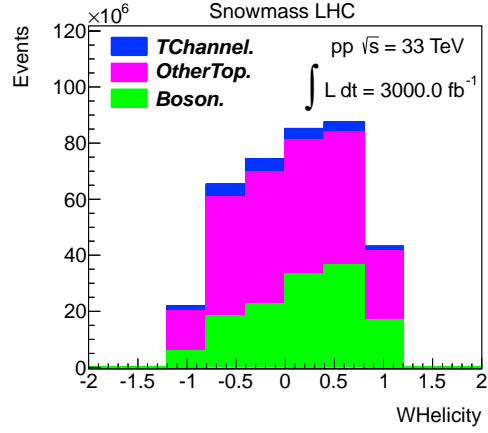


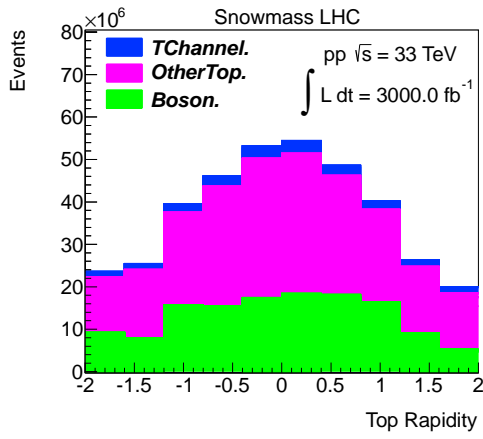
FIG. 2: Kinematic distributions for  $300 \text{ fb}^{-1}$  at 14 TeV: (a) transverse mass of the  $W$  boson, (b) helicity of the  $W$  boson, (c) rapidity of the top quark and (d) invariant mass of all the jets in the event.



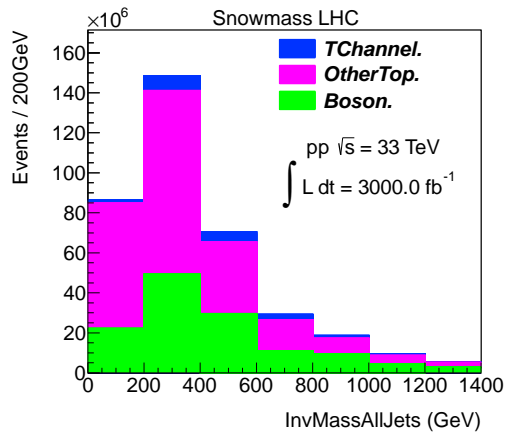
(a)



(b)



(c)



(d)

FIG. 3: Kinematic distributions for  $3000 \text{ fb}^{-1}$  at 33 TeV: (a) transverse mass of the W boson, (b) helicity of the W boson, (c) rapidity of the top quark and (d) invariant mass of all the jets in the event.

57 **IV. EVENT SELECTION**

58 To improve signal to background ratio events are required to pass the following selection  
 59 cuts for 300 fb<sup>-1</sup> at 50 pile up:

Leading non- <i>b</i> -jet $\eta$	$ \eta_\ell $	$\geq 3.0,$
Top Mass	$160 \text{ GeV} \leq M_{top} \leq 180 \text{ GeV},$	
Top P <sub>T</sub>	$T_{pt}$	$\geq 70 \text{ GeV}$
Top Polarization Optimal Basis	$T_{pol}$	$\geq 0$
Scalar $H_T$	$H_T$	$\leq 300 \text{ GeV}$

(2)

60 For the 3000 fb<sup>-1</sup> scenario at 14 TeV, the same selection cuts are used except the  $H_T$   
 61 cut, which is loosened to  $H_T \leq 360 \text{ GeV}$ .

62 In the case of 33 TeV, the preselection is slightly modified increasing the lepton  $p_T$  cut  
 63 from 40 to 50 GeV and increasing the jet  $p_T$  cut from 70 to 75 GeV. Moreover the final  
 64 selection includes modifications of the same cuts as well as the addition of leading non-*b*-jet  
 65  $p_T \geq 100 \text{ GeV}$ . The  $H_T$  cut has been loosened to 550 GeV, the top polarization cut is  
 66 tightened to 0.2, and the top  $p_T$  cut has been tightened to 100 GeV. These differences select  
 67 a kinematic region with the highest signal to background ratio while maintaining sensible  
 68 cuts based on expected *t*-channel kinematics.

69 Figures 4 and 5 show the effect of the cuts for the 300 fb<sup>-1</sup> 14 TeV sample. For each  
 70 histogram, all cuts are applied except on the variable shown. Figures 6 and 7 show the same  
 71 for 33 TeV.

72 AT 14 TeV it is clearly visible that the most powerful variables to cut on are the leading  
 73 non-*b*-jet  $\eta$  and  $H_T$ , whereas the top mass,  $p_T$  and polarization only add some additional  
 74 discrimination. At 33 TeV, the distributions are broader and the available statistics are  
 75 lower, but the leading non-*b*-jet  $\eta$  and  $p_T$  are powerful variables again, whereas now the  
 76 separation power of  $H_T$  is limited.

77 Tables III, IV and V show the number of events passing each cut for 50 pile up at 14 TeV,  
 78 140 pile up at 14 TeV, and 140 pile up at 33 TeV respectively. The signal contribution over  
 79 the total background after all cuts is about 7.3 for 50 pile up at 14 TeV, 8.2 for 140 pile  
 80 up at 14 TeV, and 5.9 for 140 pile up at 33 TeV. The number of expected *t*-channel signal

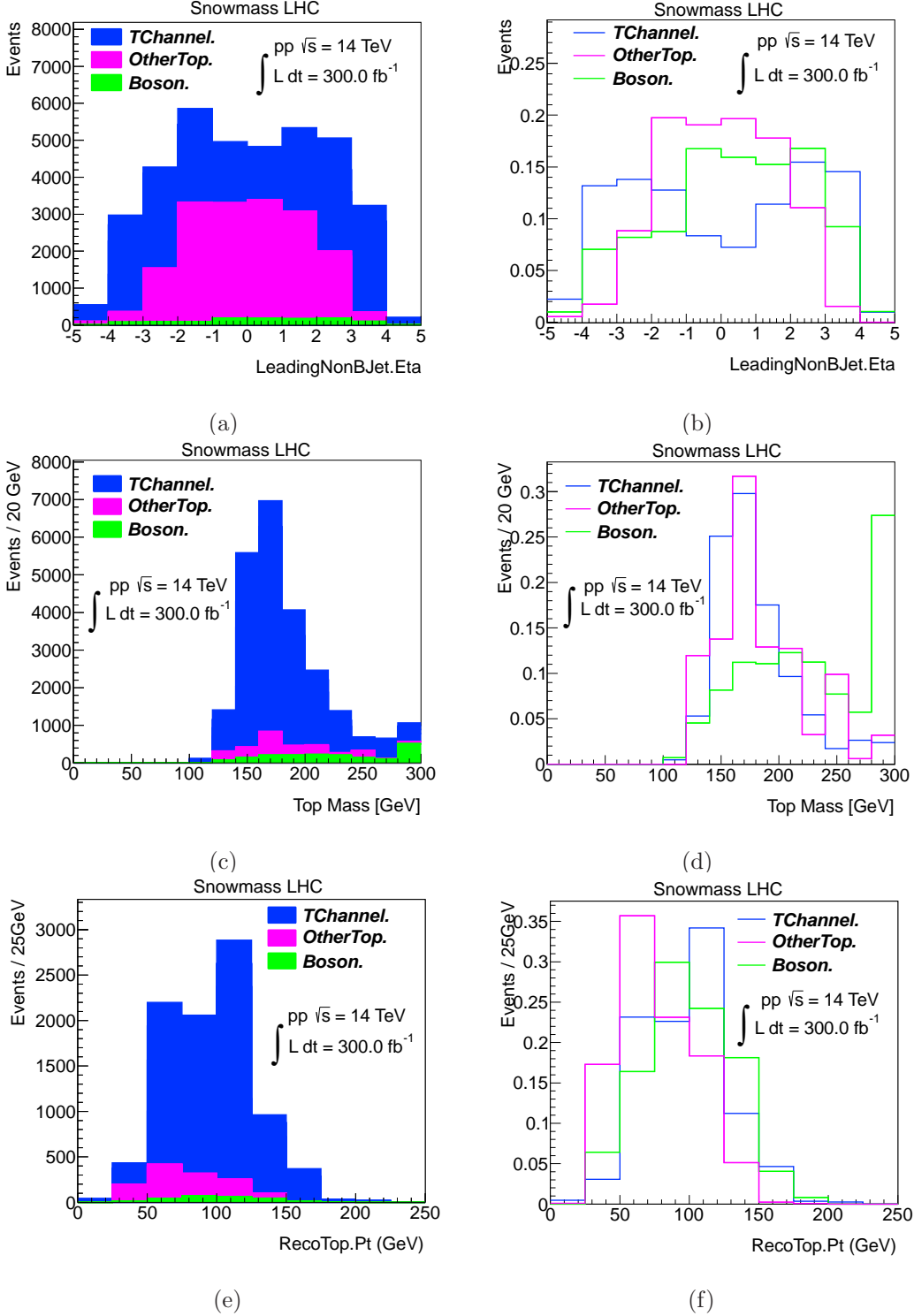


FIG. 4: Discriminant variables after all cuts have been applied except on the variable shown for  $300 \text{ fb}^{-1}$  at  $14 \text{ TeV}$ : (a, b)  $\eta$  of the leading non- $b$ -jet, (c, d)  $p_T$  of the leading non- $b$ -jet, and (e, f) mass of the top quark. Figures (a), (c) and (e) are normalized to the expected event yield while (b), (d) and (f) are normalized to unit area.

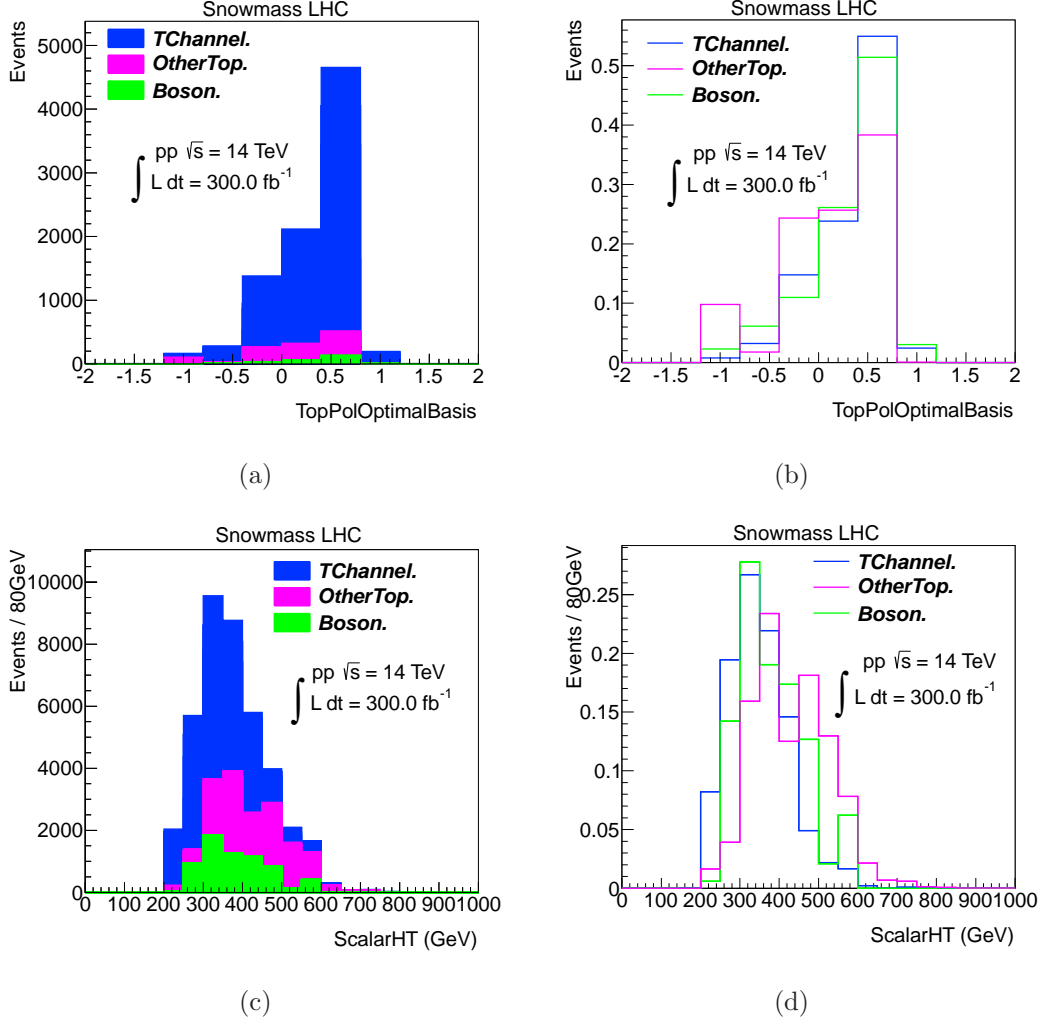


FIG. 5: Discriminant variables after all cuts have been applied except on the variable shown for  $300 \text{ fb}^{-1}$  at  $14 \text{ TeV}$ : (a, b)  $p_T$  of the top quark, (c, d) polarization of the top quark, and (e, f) scalar sum of all  $p_T$  objects. Figures (a) and (c) are normalized to the expected event yield while (b) and (d) are normalized to unit area.

81 events is 6000, 9000, and 14000, respectively. These are large, clean event samples suitable  
 82 for further single top studies.

83 A  $t$ -channel cross-section measurement can be extracted in a simple analysis by assuming  
 84 that the background is estimated with a large systematic uncertainty of 30% that accounts  
 85 for both detector modeling (including jet energy scale and pileup and  $b$ -tagging) and theory  
 86 uncertainties. No systematic uncertainty is assigned to the signal. The resulting signal  
 87 uncertainty is then added in quadrature with the statistical uncertainty to give the total  
 88 expected uncertainty shown in Table VI.

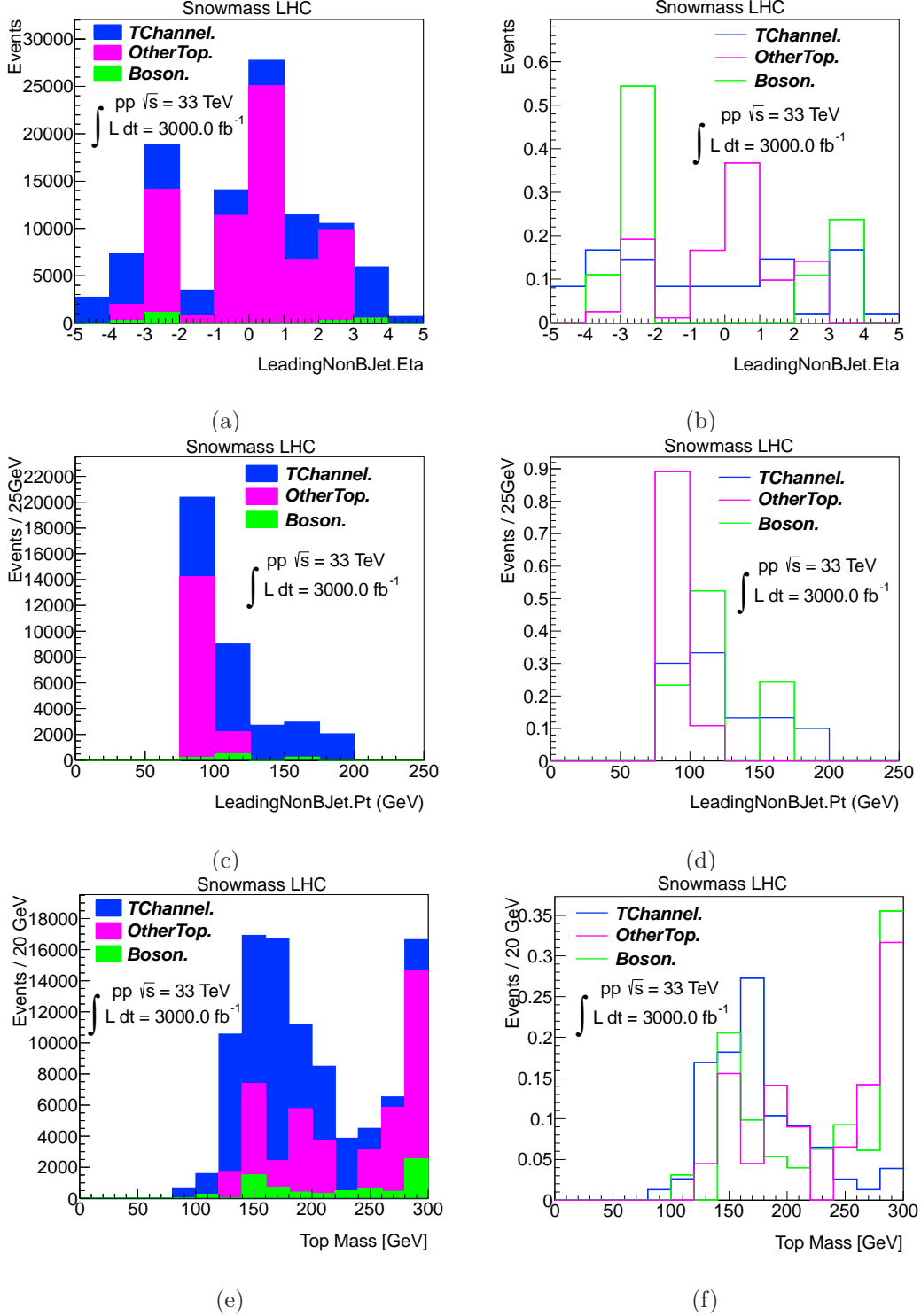


FIG. 6: Discriminant variables after all cuts have been applied except on the variable shown for  $3000 \text{ fb}^{-1}$  at 33 TeV: (a, b)  $\eta$  of the leading non- $b$ -jet, (c, d)  $p_T$  of the leading non- $b$ -jet, and (e, f) mass of the top quark. Figures (a), (c) and (e) are normalized to the expected event yield while (b), (d) and (f) are normalized to unit area.

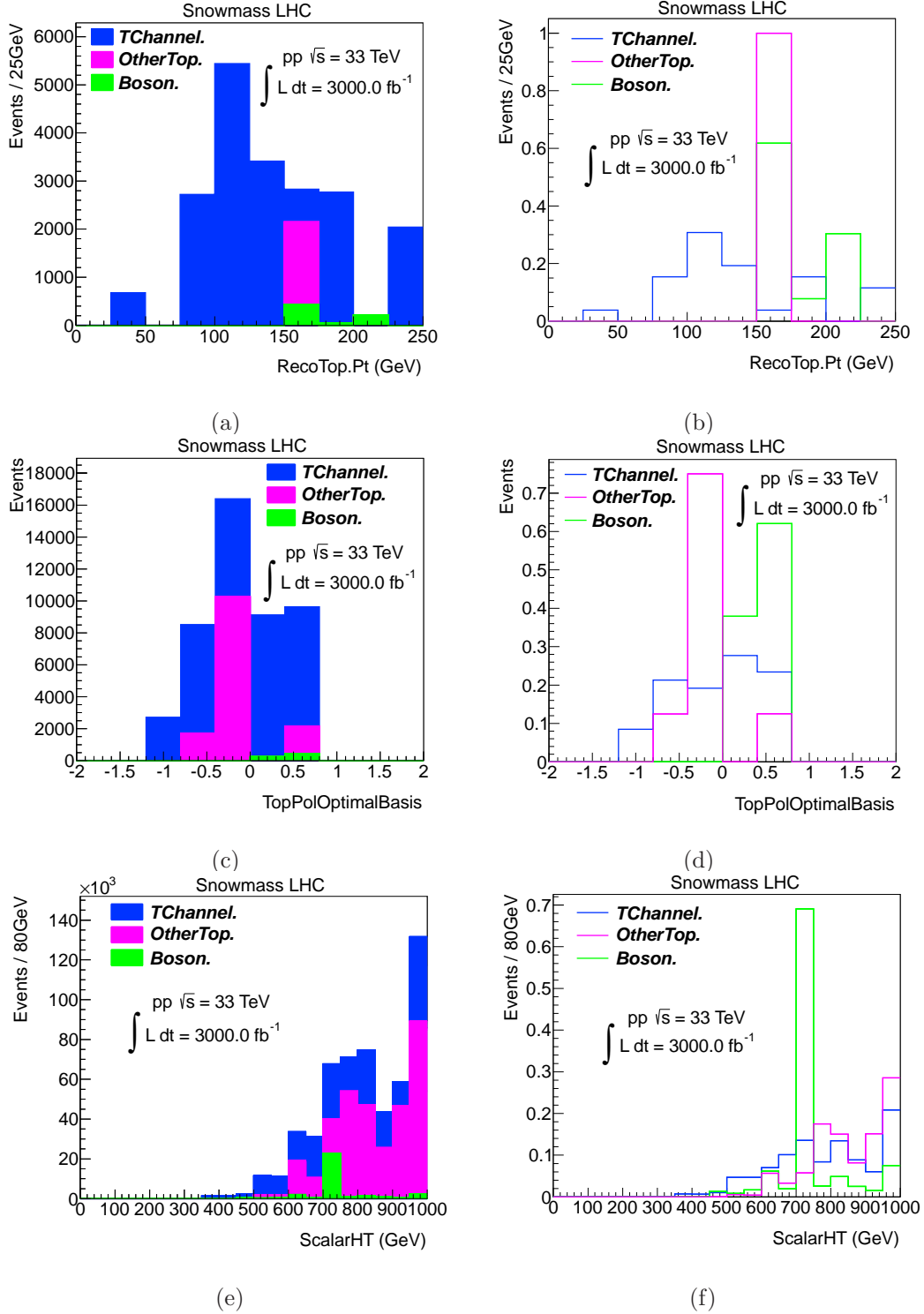


FIG. 7: Discriminant variables after all cuts have been applied except on the variable shown for  $3000 \text{ fb}^{-1}$  at  $33 \text{ TeV}$ : (a, b)  $p_T$  of the top quark, (c, d) polarization of the top quark, and (e, f) scalar sum of all  $p_T$  objects. Figures (a) and (c) are normalized to the expected event yield while (b) and (d) are normalized to unit area.

TABLE III: Cutflow of signal and background yields in 300 fb<sup>-1</sup> at 14 TeV.

Event Yield	Signal	$Wt$	$t\bar{t}$	diboson	$W + \text{jets}$	Total Background
no cuts	1.81e+07	2.10e+07	2.14e+08	1.09e+08	3.62e+07	3.80e+08
+ preselection	746000	439000	5.01e+06	122000	102000	5.67e+06
+ Leading non- $b$ -jet $\eta$	159000	13900	187000	3850	20200	226000
+ Top mas window	33600	1460	25700	105	1060	28300
+ Top $p_T$	29300	1270	22100	97.8	964	24400
+ Top Polarization	22100	700	10600	74.3	769	12100
+ $H_T$	6120	57.4	570	12.5	197	836

TABLE IV: Cutflow of signal and background yields in 3000 fb<sup>-1</sup> at 14 TeV.

Event Yield	Signal	$Wt$	$t\bar{t}$	diboson	$W + \text{jets}$	Total Background
no cuts	1.81e+08	2.10e+08	2.13e+09	1.09e+09	3.62e+08	3.79e+09
+ preselection	7.46e+06	4.23e+06	4.96e+07	1.22e+06	1.04e+06	5.61e+07
+ Leading non- $b$ -jet $\eta$	1.68e+06	189000	2.57e+06	52800	201000	3.01e+06
+ Top mas window	306000	17400	274000	2580	9970	304000
+ Top $p_T$	263000	14300	229000	2530	8870	255000
+ Top Polarization	189000	8180	125000	481	6980	140000
+ $H_T$	9380	115	672	0.0	345	1130

TABLE V: Cutflow of signal and background yields in  $3000 \text{ fb}^{-1}$  at 33 TeV.

Event Yield	Signal	$Wt$	$t\bar{t}$	diboson	$W + \text{jets}$	Total Background
no cuts	2.52e+09	9.88e+08	1.13e+10	2.70e+09	8.28e+08	1.59e+10
+ preselection	1.66e+07	1.25e+07	1.60e+08	4.30e+06	2.04e+06	1.79e+08
+ Leading non- $b$ -jet $\eta$	5.25e+06	1.51e+06	1.98e+07	458000	585000	2.23e+07
+ Leading non- $b$ -jet $p_T$	3.74e+06	557000	8.13e+06	190000	426000	9.30e+06
+ top mas window	666000	47000	1.00e+06	10000	16800	1.07e+06
+ top Pt	595000	33000	842000	9200	14300	898000
+ Top Polarization	184000	8700	237000	2250	7970	256000
+ $H_T$	14200	0.0	1710	54.0	650	2410

Collider	statistical uncertainty [%]	systematic uncertainty [%]	total uncertainty [%]
$300\text{fb}^{-1}$ , 14 TeV	1.4	4.1	4.3
$3000\text{fb}^{-1}$ , 14 TeV	1.1	3.6	3.8
$3000\text{fb}^{-1}$ , 33 TeV	0.9	5.1	5.2

TABLE VI: Estimated  $t$ -channel cross section precision assuming a 30% background systematic uncertainty.

89 Even though the relative background uncertainty is large, the signal cross-section can  
90 still be measured with high precision because the selected sample consist almost entirely of  
91  $t$ -channel signal events. The signal precision improves at the high-luminosity LHC due to  
92 the larger event sample.

93 Figures 8 and 9 show kinematic distributions after all cuts for  $300 \text{ fb}^{-1}$  at 14 TeV and  
94  $3000 \text{ fb}^{-1}$  33 TeV, respectively.

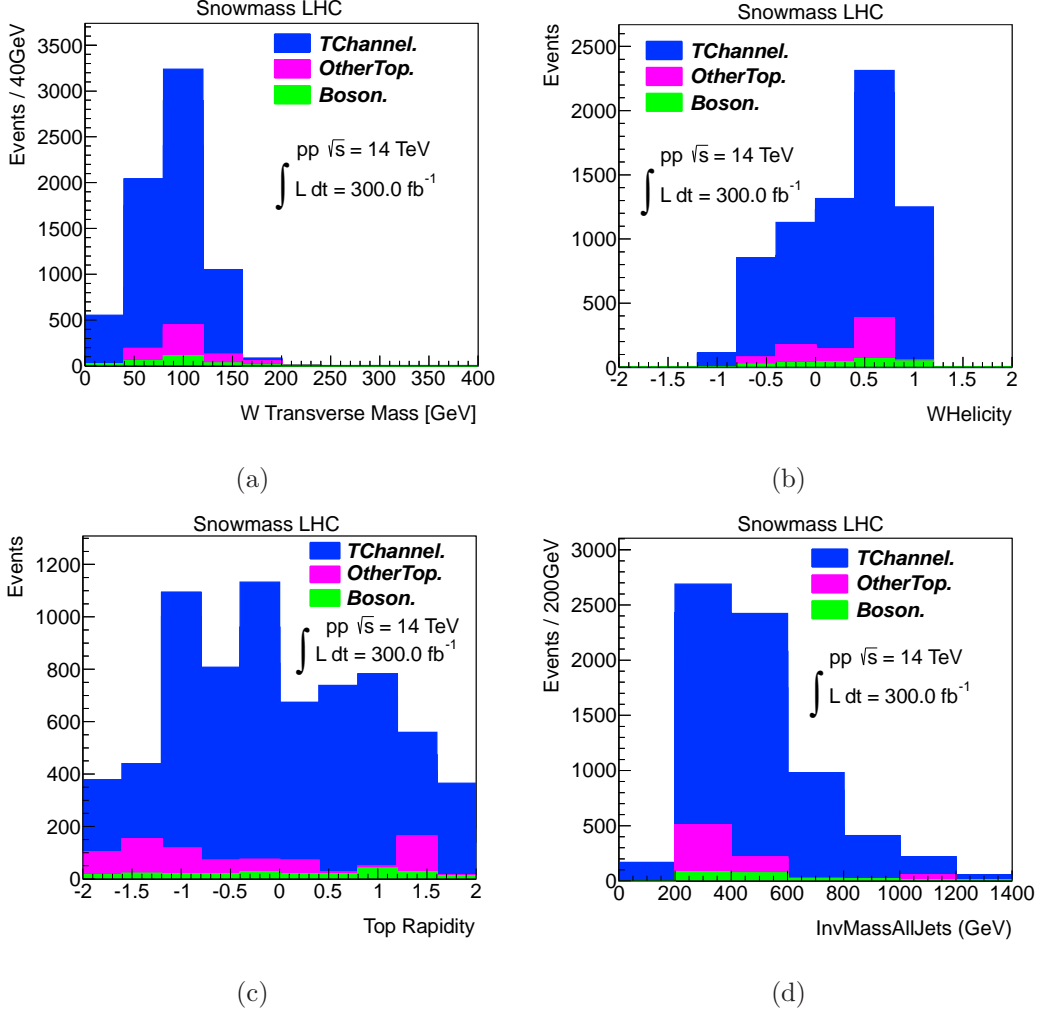


FIG. 8: Kinematic distributions for events passing selection cuts for  $300 \text{ fb}^{-1}$  at 14 TeV: (a) transverse mass of the W boson, (b) helicity of the W boson, (c) rapidity of the top quark and (d) invariant mass of all the jets in the event.

## 95 V. CONCLUSIONS

96 We have presented the *t*-channel single top quark production cross-section measurement  
 97 for three scenarios, studied within the context of the Snowmass energy frontier group:  
 98  $300 \text{ fb}^{-1}$  of 14 TeV *pp* data with an average pileup of 50 events,  $3000 \text{ fb}^{-1}$  of 14 TeV  
 99 *pp* data with an average pileup of 140 events, and  $3000 \text{ fb}^{-1}$  of 33 TeV *pp* data. For each  
 100 the appropriate Snowmass detector models are used. The *t*-channel events are selected in  
 101 the lepton+jets top quark decay mode. The background consists mainly of *W*+jets and top  
 102 quark pair events. The *t*-channel signal is isolated through a series of cuts, resulting in large,

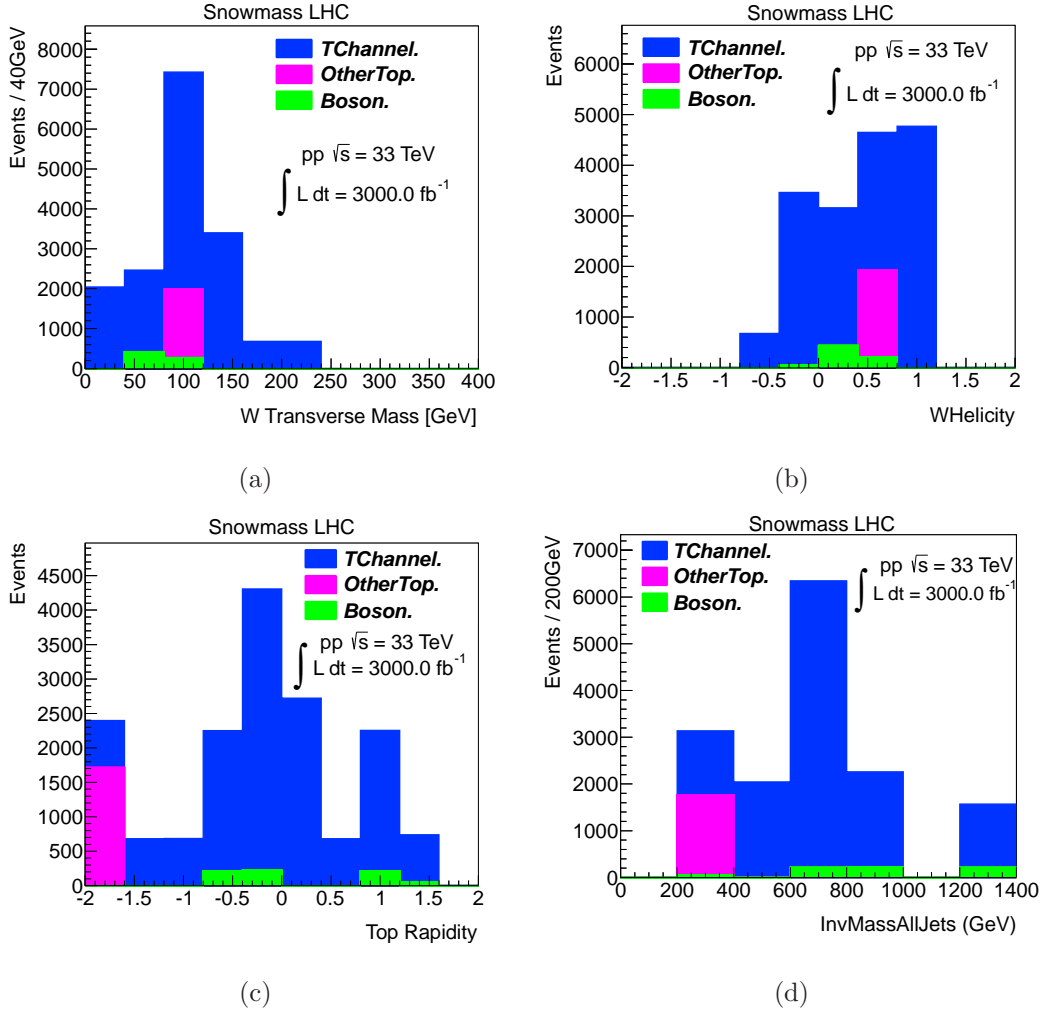


FIG. 9: Kinematic distributions for events passing selection cuts for  $3000 \text{ fb}^{-1}$  at 33 TeV: (a) transverse mass of the W boson, (b) helicity of the W boson, (c) rapidity of the top quark and (d) invariant mass of all the jets in the event.

103 pure event samples. The expected  $t$ -channel cross-section precision is about 5% or better.

## Acknowledgments

We acknowledge the support of the entire Snowmass effort, in particular the samples provided by the energy frontier. This work was supported in part by the U.S. National Science Foundation under Grants No. PHY-0952729 and PHY-1068318.

- 
- [1] G. Aad et al. (ATLAS Collaboration), *Phys.Lett.* **B716**, 1 (2012), 1207.7214.
  - [2] S. Chatrchyan et al. (CMS Collaboration), *Phys.Lett.* **B716**, 30 (2012), 1207.7235.
  - [3] Tevatron Electroweak Working Group (CDF Collaboration, D0 Collaboration) (2009), 0908.2171.
  - [4] T. Aaltonen et al. (CDF Collaboration), *Phys. Rev. Lett.* **103**, 092002 (2009), 0903.0885.
  - [5] V. M. Abazov et al. (D0 Collaboration), *Phys. Rev. Lett.* **103**, 092001 (2009), 0903.0850.
  - [6] CDF Collaboration, CDF/PUB/TOP/PUBLIC/10793 (2012), URL [http://www-cdf.fnal.gov/physics/new/top/confNotes/cdf10793\\_SingleTop\\_7.5\\_public.pdf](http://www-cdf.fnal.gov/physics/new/top/confNotes/cdf10793_SingleTop_7.5_public.pdf).
  - [7] D0 Collaboration, *Phys.Lett.* **B705**, 313 (2011), 1105.2788.
  - [8] ATLAS Collaboration (2012), 1205.3130.
  - [9] CMS Collaboration (2012), 1209.4533.
  - [10] CMS Collaboration, CMS-PAS-TOP-12-38 (2013).
  - [11] ATLAS Collaboration, ATLAS-CONF-2012-132 (2013).
  - [12] CMS Collaboration, CMS-PAS-TOP-12-011 (2013).
  - [13] J. Alwall, M. Herquet, F. Maltoni, O. Mattelaer, and T. Stelzer, *JHEP* **1106**, 128 (2011), 1106.0522.
  - [14] MadAnalysis 5 - A package for event file analysis, [madanalysis.irmp.ucl.ac.be](http://madanalysis.irmp.ucl.ac.be) (2013).
  - [15] T. Sjöstrand et al., *Computer Phys. Commun.* **135**, 238 (2001), hep-ph/0010017.
  - [16] Pythia/pgs package for MadGraph, [launchpad.net/pythia-pgs-for-mg](http://launchpad.net/pythia-pgs-for-mg) (2011).
  - [17] De Favereau J., Delaere C., Demin P., Giammanco A., Lematre V., Mertens A., Selvaggi M. (2013), 1307.6346.
  - [18] Snowmass Energy Frontier twiki page (2013), <http://www.snowmass2013.org/tiki-index.php?page=Energy+Frontier>.